Biomacromol. J., Vol.12, No.1, 51-68, January 2026.

Biomacromolecular Journal

www.bmmj.org

Advances in superoxide dismutase biomimetic nanozymes: Catalytic functions and therapeutic potentials

Hoda Zamanian Dastmalchi, Fariba Dashtestani, Kimia Kermanshahian, Hedayatollah Ghourchian*

Laboratory of Bioanalysis, Institute of Biochemistry and Biophysics, University of Tehran, Tehran, Iran

(Received 5 February 2023, Accepted 14 May 2023, Published 30 January 2026)

ABSTRACT

Superoxide dismutase (SOD) nanozymes have emerged as promising synthetic alternatives to natural SOD enzymes, offering enhanced stability, tunable catalytic activity, and cost-effective production. This review comprehensively categorizes SOD-mimetic nanozymes, including metal oxide-based, metal-based, metal-organic frameworks, hybrid nanozymes, carbon-based nanomaterials, and single-atom nanozymes. The catalytic mechanisms of these nanozymes are discussed, emphasizing their ability to mimic the redox cycling of natural SOD by scavenging superoxide radicals ($O_2^{\bullet -}$) and converting them into less harmful species (O_2 and H_2O_2). Key advantages of SOD nanozymes include their multi-enzyme mimicry (e.g., catalase, peroxidase, oxidase activities), biocompatibility, and applications in biomedicine such as antioxidant therapy, cancer treatment, and neuroprotection, biosensing, and environmental remediation. However, challenges such as immunogenicity, cytotoxicity, specificity, and catalytic efficiency still need further optimization. Future research should focus on mechanistic elucidation, scalable synthesis, and clinical translation to harness the full potential of SOD nanozymes in addressing oxidative stress-related diseases and industrial applications.

Keywords: Enzyme mimic, reactive oxygen species, antioxidant therapy, mechanisms, biomedical applications

INTRODUCTION

The discovery of peroxidase-like activity of ferromagnetic nanoparticles challenged the long-standing notion that inorganic materials are biologically inert, initiating a new era in nanozyme research. Since then, over 300 nanomaterials have been identified with intrinsic enzyme-like activities, collectively termed nanozymes. These artificial enzymes combine the structural advantages of nanomaterials with the catalytic efficiency of biological enzymes, exhibiting high stability, tunable activity, and multifunctionality. Unlike natural enzymes, nanozymes maintain catalytic performance under harsh or physiological conditions, enabling their application across industrial catalysis, biosensing, environmental remediation, and biomedicine [1–3].

Recent advances in nanotechnology have expanded the biomedical relevance of

nanozymes, which often display multi-enzyme mimetic activities (e.g., oxidoreductase, hydrolase, and superoxide dismutase). Their nanoscale dimensions, modifiable surfaces, and large specific areas facilitate selective interactions with biomolecules, supporting applications in diagnostics, imaging, tissue engineering, and drug delivery [4]. Among reactive oxygen species (ROS), the superoxide radical ($O_2^{\bullet -}$) is a primary source of oxidative stress, contributing to neurodegenerative, cardiovascular, and neoplastic disorders [5]. Superoxide dismutases (SODs) are metalloenzymes that catalyze the dismutation of $O_2^{\bullet -}$ into O_2 and H_2O_2, providing the first line of defense against oxidative damage [6]. Figure 1. Shows catalytic reaction of natural and mimetic SOD function. Also, SODs' clinical and industrial use is limited by poor stability, high production cost, and short half-life [7]. Although SODs are explored in medicine, cosmetics, and food industries, challenges such as low bioavailability and membrane permeability hinder their therapeutic translation. To overcome these issues, various SOD mimetics have been engineered to enhance stability and catalytic efficiency [6]. In this context, SOD-mimetic nanozymes have emerged as promising alternatives, replicating natural SOD activity through redox-active centers embedded in nanostructures. They utilize diverse materials—metal oxides (e.g., CeO_2, MnO_2, Fe_3O_4), noble metals (Au, Pt), metal–organic frameworks (MOFs), and carbon-based nanostructures—to scavenge ROS efficiently [8]. Some of them exhibit multi-enzyme functionality, enabling synergistic antioxidant effects that go beyond SOD catalysis [9]. Unlike other common nanozymes (catalase, peroxidase, oxidase), SOD-mimetic nanozymes specifically target superoxide radicals, addressing the root cause of oxidative damage [10]. Natural SODs (e.g., Cu/Zn-, Mn-, Fe-SODs) are metalloproteins produced through recombinant expression, while synthetic SOD nanozymes feature redox-active centers distributed across nanostructured surfaces. This design flexibility allows fabrication of single-atom catalysts, MOF-based systems, or metal nanoparticles, providing tunable and robust SOD-like performance [8].

This review highlights the classification, mechanisms, and biomedical applications of SOD nanozymes, emphasizing their potential in therapeutics, diagnostics, and environmental remediation. Remaining challenges such as biocompatibility, selectivity, and scalability are discussed, alongside future perspectives to advance their clinical translation. By integrating nanotechnology and enzymology, SOD-mimetic nanozymes offer a powerful strategy for combating oxidative stress–related diseases.

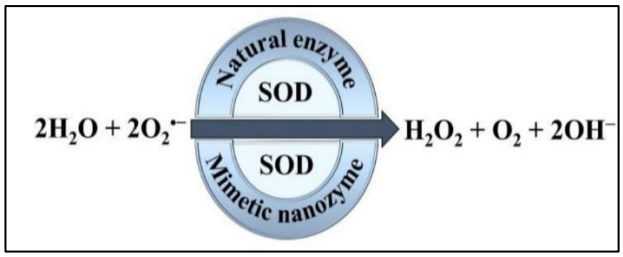

Figure 1. The scheme for catalytic reaction of natural and mimetic SOD function.

Categories of mimetic SODs

Metal Oxide-Based Nanozymes

Metal oxide-based nanozymes exhibit the enzyme-like catalytic behavior arising from redox-active surface metal centers. This activity proceeds through reversible electron-transfer cycling between adjacent oxidation states ($M^n \leftrightarrow M^{n+1}$). The process involves sequential oxidation and reduction steps mediated by surface defects, oxygen vacancies, and the redox-state ratio (e.g. Ce^{3+}/Ce^{4+}, Fe^{2+}/Fe^{3+}) [11].

Cerium Oxide Nanoparticles

Cerium oxide nanoparticles (CeO_2 NPs, nanoceria) are rare-earth metal oxides with

remarkable redox flexibility due to the coexistence of Ce^{3+} and Ce^{4+} oxidation states. Their fluorite cubic lattice accommodates oxygen vacancies that act as active catalytic sites. The reversible Ce^{3+}/Ce^{4+} transition enables dynamic redox cycling between Ce_2O_3 and CeO_2 phases, crucial for free radical scavenging. Nanoceria are commonly synthesized through hydrothermal, precipitation, sol–gel, or combustion methods, with size, shape, and Ce^{3+} ratio being tunable by precursor concentration, pH, and temperature. Smaller nanoparticles with higher surface area display enhanced oxygen vacancy density and superior catalytic performance [12].

Nanoceria have demonstrated broad potential across multiple fields: i) Biomedical: antioxidant therapy, neuroprotection, anti-inflammatory treatments, wound healing, radioprotection, and biosensing. ii) Industrial/environmental: UV-blocking additives, fuel cell catalysts, pollutant degradation, and oxygen sensors. iii) Their biocompatibility and regenerative catalytic nature make them suitable for continuous oxidative stress regulation in biological and industrial systems [13]. The SOD-mimetic activity of nanoceria was first reported by Self et al. (2007), who demonstrated its ability to catalyze O2•– dismutation. The mechanism involves the redox cycling between Ce^{3+} and Ce^{4+} centers. At first, Ce^{3+} donates an electron to O2•–, forming H_2O_2 and converting to Ce^{4+}. Then, Ce^{4+} is reduced back to Ce^{3+} through H_2O_2 decomposition, mimicking catalase activity. This coupled process allows auto-regeneration of active sites and simultaneous scavenging of both O2•– and H_2O_2. Figure 2. illustrates the steps of SOD-mimic catalytic mechanism of nanoceria [14]. Reported kinetic parameters vary with synthesis and surface chemistry, with Km values ranging from 0.1–1.2 mM and Vmax around 10^{-6}–10^{-5} M. s^{-1}, comparable to native SOD enzymes. Doping with metals (e.g., Cr) increases the Ce^{3+} fraction and enhances activity up to 3–5 fold [15].

The nanoceria exhibited exceptional redox reversibility, structural stability, long-term catalytic regeneration, and multi-enzyme (SOD-catalase-, and oxidase-like) activity. Future directions focus on biocompatible coatings, doping strategies (e.g., Cr, Gd, Au composites), and surface functionalization (e.g., ferritin or polymer encapsulation) to optimize stability, selectivity, and targeted delivery. Continued research into size, valence, and activity correlations will further enhance nanoceria's role in biomedical and catalytic applications [11].

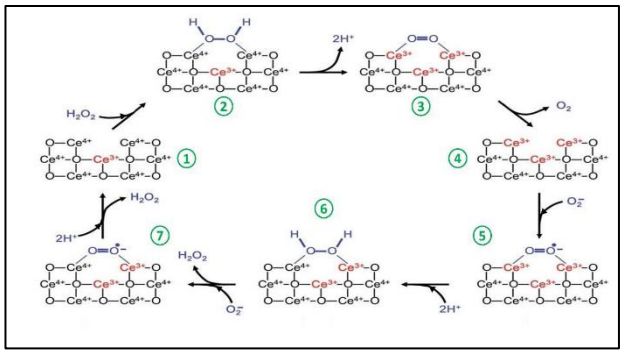

Figure 2. Seven steps of SOD-mimic catalytic mechanism of nanoceria. Reproduced with permission of [14] Copyright 2023., RSC

So far, plenty of cerium compounds have been synthesized among them cerium vanadate [12], Au@CeO2 [16,17], cerium oxide@montmorillonite [18], cerium oxide@cyclodextrin [19–23], ceria-integrated microneedles [24], Au@Ce [25], cerium oxide-gadolinium [26], citric acid-stabilized nanoceria [27], polymer-coated nanoceria [28] showed remarkable enzymatic properties.

Manganese Oxide Nanoparticles

In natural SOD enzymes, manganese catalyzes the dismutation of superoxide radicals ($O_2^{\bullet-}$) into O_2 and H_2O_2 as part of the cellular

antioxidant defense system. Bulk manganese and its simple salts show limited SOD-like activity due to slow electron-transfer kinetics and restricted redox flexibility. In contrast, manganese oxide nanozymes (MnO_x NPs) display significantly enhanced catalytic performance through nanoscale effects and redox cycling among $Mn^{2+}/Mn^{3+}/Mn^{4+}$ states. The high surface area, oxygen vacancies, and abundant active sites facilitate efficient adsorption and conversion of superoxide anions [29]. Beyond SOD-like activity, MnO nanoparticles also exhibit catalase (CAT)-mimetic behavior by decomposing H_2O_2, one of the SOD reaction products, into O_2, thereby amplifying their antioxidative capacity. This dual functionality enables MnO-based nanozymes to simultaneously scavenge $O_2^{\bullet-}$ and H_2O_2, both implicated in tumor progression. Consequently, MRI contrast-enhanced MnO nanoparticles have been proposed for combined tumor imaging and therapy. Notably, Barnes et al. reported that free Mn^{2+} ions also display SOD-mimetic activity, but with a rate constant ($kSOD = 6.1 \times 10^7\ M^{-1}\cdot s^{-1}$) approximately half that of MnO nanoparticles (Figure 3) [30].

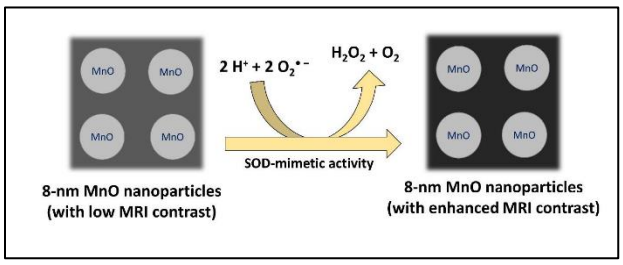

Figure 3. The effect of SOD-mimetic activity of MnO NPs on MRI image contrast. Redrawn based on [29].

The MnO_x NPs also mimics the catalytic cycle of natural SOD enzymes by effectively dismutating $O_2^{\bullet-}$ into O_2 and H_2O_2 through the reversible switching of oxidation states ($Mn^{4+} \leftrightarrow Mn^{3+}/Mn^{2+}$) by surface Mn atoms. Furthermore, an active catalytic environment that is not present in bulk materials is produced by the crystal structure, surface oxygen vacancies, and electron transfer dynamics of MnO_2 nanoparticles. Since the redox cycling between Mn^{2+}/Mn^{3+} states are not effectively facilitated in the absence of an optimized catalytic surface or appropriate electron transfer pathways, bulk manganese or its simple compounds (such as Mn^{2+} salts) typically exhibit limited or negligible intrinsic SOD-like activity. Manganese peroxide (MnO_2) nanozymes, on the other hand, exhibit strong SOD-mimetic activity because of their high surface area, nanoscale size, and surface defect sites that boost redox reactivity [31]. Overall, manganese oxide nanozymes represent a promising class of multifunctional materials with potent SOD-like activity and broad potential in biomedical, environmental, and energy-related applications. Examples include MnO_2–ferritin (MnO_2–FTn) fentozyme [32], MnO_2@graphene oxide (MnO_2@GO) [33], and PEGylated Mn_3O_4 nanoparticles [34], which demonstrate tunable catalytic and therapeutic performance.

Iron Oxide Nanoparticles

Iron oxide nanoparticles (Fe_3O_4 NPs) are magnetic nanoparticles with notable redox flexibility due to the coexistence of Fe^{2+} and Fe^{3+} ions in their crystal lattice. Their high surface area to volume ratio enables efficient interaction with ROSs. Fe_3O_4NPs are commonly synthesized through co-precipitation, hydrothermal, sol–gel, thermal decomposition, or microemulsion methods, which allow control over size, shape, and magnetic properties [35]. Fe_3O_4 NPs have demonstrated potential in various biomedical and industrial applications. In the biomedical field, they have been explored for antioxidant therapy, drug delivery, magnetic resonance imaging (MRI) contrast enhancement, hyperthermia treatment, biosensing, and diagnostics. Industrially, they have been utilized in catalysis, wastewater

treatment, and magnetic separation processes. The combination of their magnetic properties and biocompatibility makes Fe_3O_4 NPs versatile for both therapeutic and industrial applications [36]. Fe_3O_4 NPs also can mimic SOD activity by scavenging superoxide radicals through redox reactions of Fe^{2+}/Fe^{3+} ions. Iron ions in Fe_3O_4 NPs undergo redox cycling with superoxide radicals, neutralizing them. They catalyze the dismutation of superoxide radicals into less harmful oxygen and hydrogen peroxide. After reacting with superoxide radicals, Fe_3O_4 NPs are regenerated, allowing continuous antioxidant activity. Reported kinetic parameters vary depending on synthesis methods, surface modification, and particle size. Fe_3O_4 NPs exhibit effective scavenging at concentrations comparable to natural SOD [37].

Fe_3O_4 NPs offer several advantages, including efficient O2•– scavenging, regenerative SOD-like activity, high surface area, and magnetic properties that enable targeted delivery and separation. However, they have limitations such as potential cytotoxicity at high doses, aggregation in physiological media, and variability in SOD-like activity based on size and surface chemistry. Future research should focus on surface functionalization for improved biocompatibility and selectivity, doping or composite formation to enhance activity, and in vivo studies to establish safety and therapeutic efficacy. Continued investigation into size–redox–activity relationships will further optimize Fe_3O_4 NPs for biomedical and catalytic applications. [38].

Nickel oxide nanomaterials

Nickel oxide nanoparticles (NiO NPs) are p-type semiconductor metal oxides that have attracted considerable attention due to their wide range of applications, including fuel cells, gas sensors, solar cells, water splitting, and electrochromic devices. Recently, NiO nanoflowers have been explored as SOD-mimetic nanozymes. The suitable redox potential of NiO nanoflowers allows them to catalyze superoxide scavenging by cycling between Ni (III) and Ni (II) oxidation states, functioning as electron-transfer mediators [39]. NiO nanoflowers exhibit a two-step mechanism for their dismutase activity. Initially, Ni (II) in the nanoflowers is oxidized to Ni (III) by transferring an electron to the first O2•–, converting it into hydrogen peroxide (H2O2). Subsequently, Ni (III) is reduced back to Ni (II) by accepting an electron from a second superoxide radical, simultaneously oxidizing it to molecular oxygen (O2). This cyclic electron transfer between Ni (II) and Ni (III) underlies the intrinsic SOD-mimetic activity of NiO nanoflowers (Figure 4), enabling continuous scavenging of O2•– [39]. Also, the SEM and TEM images of NiO-nanoflowers are illustrated in Figure 4 [40]. NiO nanoflowers are typically synthesized through hydrothermal, sol–gel, or precipitation methods, which allow control over morphology, size, and surface properties, critical factors for their catalytic performance. Their unique structure and redox cycling capability make them promising candidates for biomedical applications aimed at mitigating oxidative stress, as well as for industrial processes that benefit from their antioxidant and catalytic properties [41].

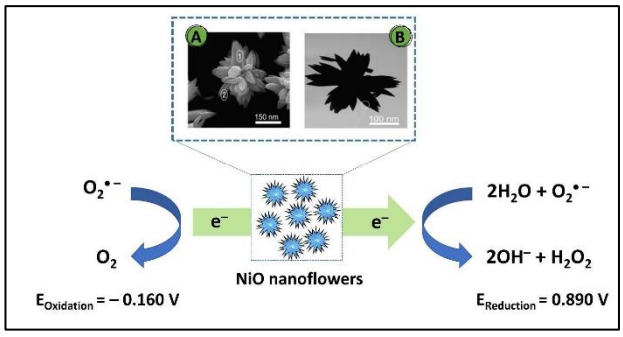

Figure 4. SOD mimetic activity of NiO-nanoflowers. Redrawn based on [13]. (A) SEM and (B) TEM images of NiO-NFs. Reprinted with permission from [18].

The advantages of NiO nanoflowers include efficient SOD-like activity, structural stability, and tunable redox properties. Limitations include potential cytotoxicity at high concentrations and variability in activity depending on size, shape, and surface chemistry. Future research may focus on surface functionalization, doping strategies, and hybrid nanocomposites to enhance biocompatibility, catalytic efficiency, and targeted application in therapeutic and diagnostic fields [39].

RuO2 nanozyme

The RuO2 nanozyme is another multi-enzyme-like activity nanozyme that has been developed to prevent acute kidney injury. The tiny RuO2 NPs (~ 2 nm) would rapidly be absorbed by human embryonic kidney cells and, consequently, reduce ROS injury. The RuO2 NPs mimic the activity of catalase, glutathione peroxidase, POD, and SOD. Additionally, the biocompatibility of RuO2 NPs makes them useful in developing biomedicine [42]. As the example Ru@V2O4 nanowires [43] and RuO2-PVP [44] were reported.

Metal-Based Nanozymes

Metal-based nanozymes constitute another significant class of SOD mimetics that exhibit remarkable catalytic efficiency due to their intrinsic redox activity and tunable surface coordination chemistry. These nanozymes are typically composed of transition or noble metals, such as manganese, copper, iron, gold, and platinum, which can efficiently cycle between multiple oxidation states to facilitate superoxide dismutation [45].

Gold Nanoparticles

The properties and catalytic activity of gold nanoparticles (GNPs) depend on their components, size, and shape. Surface modification of GNPs, such as combining with the other NPs or various protein coatings, determines the type of GNP catalytic activity and enhances it [46]. The electronic properties of AuNPs allow them to capture/release electrons when interacting in redox reactions and thus could enhance an associated redox catalyst activity. Recent research has focused on enhancing the stability and catalytic efficiency of AuNPs by surface modification and creating hybrid nanostructures with other materials like polymers and metal oxides. These advancements aim to improve their performance and expand their applicability in various fields such as medicine, environmental protection, and energy [47]. Using protoporphyrin (PpIX), a trimetallic alloy nanozyme AuCuPt-PpIX as an instance of GNPs was reported [48]. As shown in Figure 5, bis-thiocarbamate copper (II) complexes have been demonstrated as O2•– scavengers to mimic Cu/ZnSOD [21].

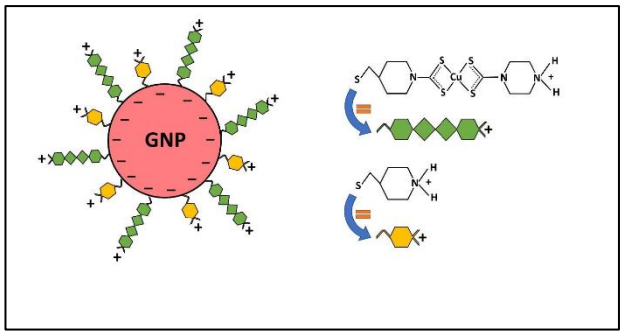

Figure 5. Schematic illustration of the double layer formed on GNPs and the protonated mixed monolayer. Redrawn based on [57].

Platinum Nanoparticles

Platinum nanoparticles (PtNPs) are a new class of SOD-mimetic antioxidants. The antioxidative activity of PtNPs is related to a direct electron transfer from ROS to the electron cloud at the surface of NPs [26,49]. PtNPs provide active sites for the adsorption and conversion of superoxide radicals (O_2^-) into oxygen (O_2) and hydrogen peroxide (H_2O_2), mimicking the natural SOD enzyme. This process is facilitated by the high surface area and reactivity of PtNPs. Platinum nanoparticles exhibit potent SOD-like

activity, making them valuable in biomedical, environmental, and energy applications. Their ability to mimic natural enzymes and participate in redox reactions underpins their diverse utility in therapeutic, catalytic, and energy storage solutions [50]. Arginine-rich peptide/platinum hybrid colloid nanoparticle cluster nanozyme [51], Pt@PVP NPs [26], PtCu nano-alloys [28], nanocomposite and bimetallic alloys of Pt-Cu [50] are instances of platinum NPs have synthesized so far. Also, integrating carbon nanodots (CNDs) with PtNPs, a novel Pt@CNDs nanocomposite was engineered as an efficient nanozyme with SOD- and catalase (CAT)-like specific activities of 12,605 U/mg and 3172 U/mg, respectively [52].

Metal-Organic Frameworks

Metal-organic frameworks (MOFs) are a class of crystalline materials composed of metal ions or clusters coordinated to organic ligands. These structures possess high surface areas, tunable pore sizes, and versatile chemical functionalities, making them promising candidates for various applications, including mimicking the activity of superoxide dismutase (SOD) [53]. Metal-organic frameworks were used for synthesizing ultra-fine and uniform NPs with superior catalytic activity. For example, Cu-Pd alloy NPs embedded in MOF and modified by PEG were synthesized and found to exhibit the POD and SOD mimic activity. This nanozyme has developed as an effective cancer treatment and subsequently belongs to nanozyme-based chemodynamic therapy because of its low side effects, biosafety, and biocompatibility. Chemodynamic therapy might produce toxic hydroxyl radicals in the tumor microenvironment, thus promoting apoptosis of tumor cells and inhibiting tumor cell growth [54]. Metal ions or clusters within the MOF structure can serve as active sites for catalyzing the dismutation of superoxide radicals. Transition metals such as copper, manganese, and cobalt are commonly used due to their ability to undergo redox reactions. The porous nature of MOFs allows for the diffusion of superoxide radicals to the metal centers, where electron transfer reactions occur. This facilitates the conversion of superoxide radicals into less harmful species such as oxygen and hydrogen peroxide. The organic ligands in MOFs can be tailored to influence the coordination environment around the metal centers, thereby optimizing their catalytic activity towards superoxide dismutation [55].

Manganese-Based MOFs

In the manganese-based MOFs, manganese ions are the metal centers, coordinated with organic ligands. Such material shows really unique properties and functionalities that are brought together by the redox activity of manganese and the tunable structure of MOFs [56]. These materials represent another promising class used in studies of catalytic efficacy [57], energy storage [57], biomedicine [58], and the remediation of environmental pollution [59].

Iron-Based MOFs

The iron ions act as a source of catalytic centers to dismute $O2^{\bullet-}$ to oxygen and hydrogen peroxide. The Fe nodes within the MOF structure serve as the primary catalytic sites, where the Fe^{2+}/Fe^{3+} redox couple enables the dismutation of $O2^{\bullet-}$ through electron transfer reactions similar to those in natural SOD enzymes. Meanwhile, the surrounding organic ligands create a well-defined coordination environment that influences the accessibility, stability, and redox potential of the iron centers. These ligands not only help to regulate the electron density around the metal sites but also contribute to the structural integrity and surface hydrophilicity of the framework. By optimizing the metal–ligand interactions and pore characteristics, Fe-MOFs can achieve enhanced

catalytic efficiency and stability, making them promising candidates for antioxidant and biomedical applications. Like all other MOFs, iron-based MOFs also have large surface areas and well-defined structures corresponding to the pores created in them. It has this structural feature that provides abundant active sites for the interaction between O2•– and the catalytic centers and can enhance SOD mimicry efficiency. Iron-based MOFs may also result in quite stable under physiological conditions so their use as SOD mimics can be repeated. Combined with their robustness and recyclability, these features render them very applicable in practical applications, mainly in biomedicine and efforts for environmental remediation. Biocompatibility is crucial, as part of the feasibility requirements of iron-based MOFs when biomedical applications [60], especially those dedicated to SOD mimics for antioxidant therapy against oxidative stress-related diseases, are under consideration [61].

Hybrid Nanozymes

A variety of materials such as metallic nanoparticles (gold, silver, platinum), metal oxides (iron oxide, manganese oxide), carbon-based nanomaterials (like graphene, carbon nanotubes), and even organic molecules, such as enzymes or enzyme mimics, can be used to construct hybrid nanozymes. The marrying of different materials, therefore goes into the integration of different catalytic functions in one nanostructure. Hybrid nanozymes combine catalytic activities of different components; therefore, owning catalytic superiority compared to each component upon individual use. Metallic nanoparticles and enzyme-like organic molecules are integrated to have superior catalytic efficiency and substrate specificity [32].

GNP/Cu- Cys nanocomposite

A nanocomposite consisting of GNP/Cu-Cys demonstrates a strong SOD-mimetic activity [22]. As discussed, the active site of Cu-Zn SOD comprises copper and zinc ions which copper participates in catalyzing O2•– and zinc contributes to organizing the enzyme structure. Additionally, the positive-charged Lys and Arg residues are located in the active site, attracting O2•–. Similarly, in GNP/Cu-Cys, the copper ions significantly catalysis O2•– and also, the GNPs and Cys make the positive cavity for attracting O2•– (Figure 6) [22]. The cyclic conversion of copper (II) to copper (I), which is the main cause of superoxide ion dismutation, is described in the following reactions [62]:

$$Cu^{2+} + O2^{\bullet-} \rightarrow O_2 + Cu^{+} \quad (10)$$

$$O2^{\bullet-} + Cu^{+} + 2H^{+} \rightarrow H_2O_2 + Cu^{2+} \quad (11)$$

GNP/Cu-Cys comprises three components for the decomposition of O2•– including copper (II), cysteine, and GNP. In the first stage, similar to natural SOD, copper (II) plays a role in the O2•– decomposition. In the second stage, cysteine plays a crucial role in superoxide dismutation [63,64].

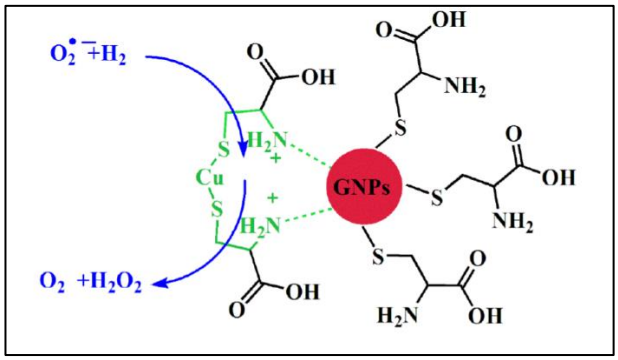

Figure 6. SOD mimetic activity of GNP/Cu-Cys nanozyme. Reprinted with permission of [42]. Copyright 2023, Springer Nature.

Au-Ag-AFT nanocomposite

A novel nanozyme composed of apoferritin containing gold-silver nanoparticles (Au-Ag-AFT) was synthesized, which exhibits peroxidase, SOD, and CAT mimetic activities [24]. As shown in Figure 7, the active site in AFT is made of six amino acid residues, including one Asp, three Glu, one His, and one glutamine Gln. In the native AFT with ferroxidase activity, the acidic amino acid residues (Glu and Asp) play a critical role in trapping and oxidizing Fe2+ ions [25]. In the Au-Ag-AFT nanozyme synthesis, acidic amino acid residues within the AFT structure play a key role. They facilitate the adsorption of metal ions (Ag+, Au3+) which are subsequently reduced by NaBH4 to Au-Ag NPs within the central cavity of the AFT protein [65]. In the second step, the His residue binds to Au-Ag NPs in the AFT cavity, where N atoms of the imidazole ring in His act as Lewis base, and Au-Ag NPs behave as Lewis acid [7]. The total charge in the AFT cavity would turn positive by these interactions and contributes to the acceleration of the catalytic process. The cavity refers to the internal hollow core of the AFT protein nanocage, which naturally serves as a confined space (~8 nm in diameter) for metal ion storage and biomineralization. As a result, this positively charged cavity improves the absorption of O2•– into the Ag-Au-AFT nanozyme [24]. Therefore, amino acids can play both structural and catalytic roles.

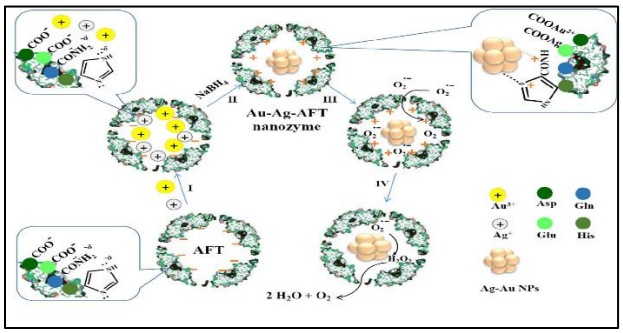

Figure 7. The process for synthesis and SOD mimetic activity of Au-Ag-AFT nanozyme. Reprinted with permission of [44]. Copyright 2023, Elsevier.

Nano-Albumin-Cu-Cys nanozyme

Lately, protein-based NPs as artificial enzymes have attracted attention due to their simple modification, easy metabolization, and biocompatibility. Nano-albumin is one of the proteins nanozymes with significant properties such as high solubility, several binding sites, long circulatory half-life, and antioxidant activity, making them an excellent drug delivery carrier [66,67]. For instance, nano-albumin from human serum has been utilized in some FDA-approved drugs such as Abraxane™ [63]. Nano-Albumin-Cu-Cys nanozyme exhibits significant SOD-like catalytic activity in scavenging $O_2^{-}\cdot$. The coordination bonding between Cu^{2+} in the Cu– Cys complex (acting as a Lewis acid) and the histidine residues of BSA (acting as a Lewis base) generates a positively charged pocket that facilitates the adsorption of O2•− [64]. Therefore, the amino acid plays catalytic role. As illustrated in Figure 8, superoxide is electrostatically adsorbed to the positively charged cavity formed by His-Cu2+, which eventually produces O2 and H2O2 [63].

Carbon-Based Nanozymes

Carbon-based nanozymes can indeed be engineered to mimic the activity of superoxide dismutase (SOD), offering an alternative approach for scavenging superoxide radicals and mitigating oxidative stress. These nanozymes are composed primarily of carbon-based materials, such as carbon nanotubes, graphene, carbon dots, and carbon nanodots [68]. Organic Se (−2 valence)-doped carbon nitride quantum dots (SegCN-QDs) nanozyme [69], Prussian blue nanozyme (PBNz) coated with polydextrose-sorbitol carboxymethyl ether (PBNz@PSC) [70], are examples of carbon-based SOD nanozymes.

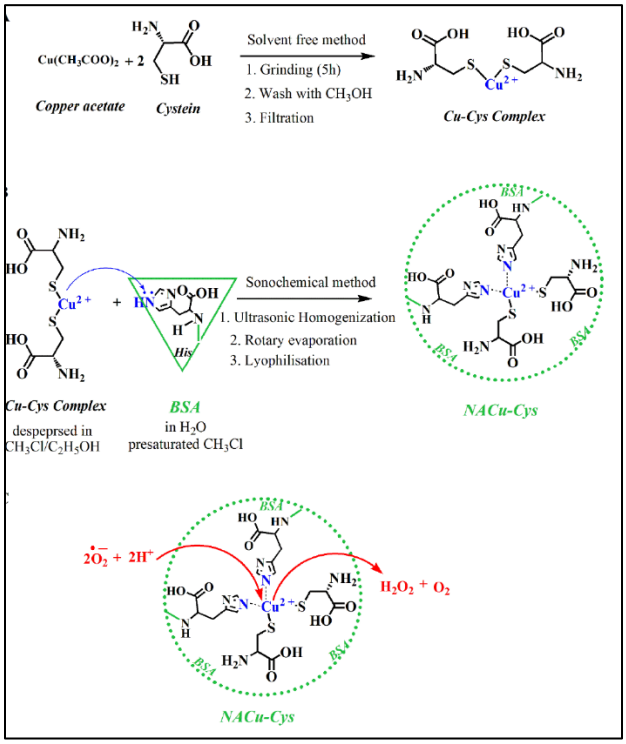

Figure 8. Schematic illustration of (A) Cu-Cys complex and (B) NACu-Cys nanozyme synthesis, and (C) SOD mimetic activity pathway of NACu-Cys. Reprinted with permission of [31]. Copyright 2023, Elsevier (NA: Nano-albumin).

Fullerene derivatives nanozyme

Fullerene derivatives have been known as the first explored nanozymes. The molecular structure of the fullerene derivatives is based on carbon nanomaterials arranged in different tube, ellipsoid, or hollow sphere forms. The most famous member of the fullerene family is the cage-like molecules composed of 60 carbon atoms (C60). The structure of C60 is shown in Figure 9-A. Similar to the natural SOD, the carboxy derivative of the C60 molecule is capable of scavenging the O2•−. Functional and structural studies on carboxy-fullerenes show that the antioxidant behavior of various compounds depends on their redox potential, degree of hydrophobicity, charge, shape, and size. Additionally, the reactivity of carboxy-fullerenes towards O2•− is influenced by dipolar moments, which are correlated with the number and position of carboxyl groups. One of the carboxy-fullerenes derivatives C3 has three carboxyl groups as malonyl connected to three C60 surface bonds (Figure 9-A). The mechanism of O2•− removal by tris-malonic acid derivative (C3) has been comprehensively investigated and illustrated in Figure 9-B [71,72].

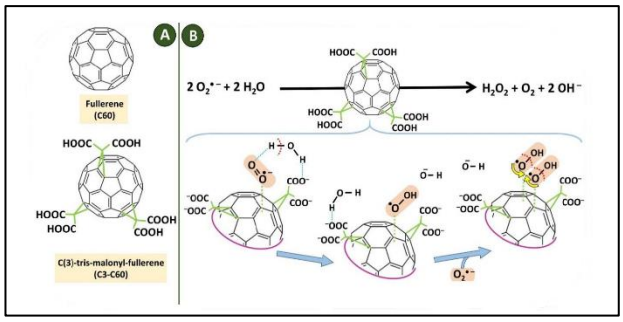

Figure 9. Schematic illustration of (A) C60 and C3-C60 structures; (B) the SOD-mimetic activity of C3-C60 for converting superoxide anion and water into hydrogen peroxide, oxygen, and hydroxyl ion. Redrawn based on [71].

Single-atom nanozymes

The focus of nanozyme research is currently on single-atom nanozymes (SAzymes), a novel class of nanozymes with the benefits of high atom utilization, high catalytic activity, cheap production cost, and great selectivity. SAzymes are also gradually being developed for the treatment of digestive diseases, such as liver cancer and cirrhosis [73], pancreatitis [74], and the control of intestinal inflammation [75]. Co/PMCS was found to have atomically dispersed ligand-unsaturated active centers and hence also possesses SOD-like, CAT-, and glutathione peroxidase activities [76]. Due to its wealth of electronic energy levels and surplus of transition metal electronic states, Au offers a strong foundation for the development of atomic-level enzymes. Au24Cd1 prioritizes the use of superoxides and significantly reduces inflammatory factors [77]. Cu-N4 SAzymes

[78], PdZn/CoSA-NC [79] are the other samples of SAzymes.

Other nanozymes

Some other nanozymes such as copper sulfide nanoclusters [80], FePO-MFs nanozyme [81], Co and Co3O4-NPs [82], porous graphene-based foam [83], PDI [84], melanin NPs [85], copper-tannic acid nanosheet [86–89], prussian blue NPs[90–97], molybdenum disulfide-based nanozymes [78,97,98], carbine nanocrystals based nanozymes [99], were also found to exhibit SOD-like activity (Table 1). Table 2 illustrates summery of intrinsic properties of SOD nanozymes such as synthesis method, applications, mechanism, kinetic values, advantages, limitations, and future directions. Also, Table 3 summarizes the kinetic values for different SOD nanozymes compared with natural SOD.

Mechanisms of natural SODs and SOD nanozymes

As shown in Figure 10, the dismutation mechanism in natural or synthetic SODs is occurred through either redox cycling or surface-mediated electron transfer. In the redox cycling mechanism, at first one O2•- is changed into O2 while reducing the metal inside the enzyme. Then, the second O2•- is converted into H2O2 while, oxidizes the M2+ back to M3. The second mechanism is based on surface-mediated electron transfer in which, the oxidation states of the noble metal nanoparticle (e.g., AuNPs, PtNPs) or carbon nanoparticle (e.g., C-dots) at the center of enzyme is remained unchanged. In this mechanism, the surface of the nanoparticle acts as an electron-conducting platform. At first, O2•- is adsorbed onto the surface of nanoparticles which facilitates the donating of an electron from one O2•- changing into O2, while the other O2•- accepts an electron to reduce to H2O2 (Figure 10-Right). The nanoparticle surface remains in the zero-valent state, simply acting as the conductor for the electron transfer [100,101].

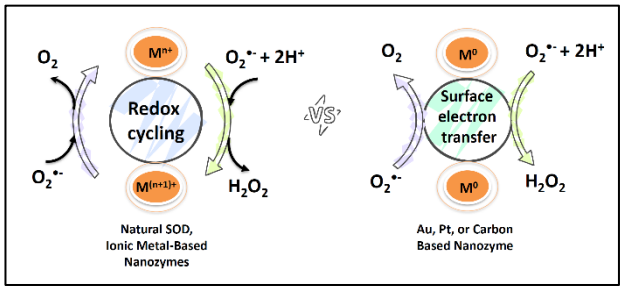

Fig. 10. Schematic representation of two mechanisms: Left, redox cycling and right, surface-mediated electron transfer for either natural SOD or SOD nanozymes.

Table 1. Other SOD-like nanozymes.

Nanozyme	Biological role	Enzyme mimetics	Ref.
Cerium vanadate	Mitochondrial depolarization inhibition Intracellular ATP level at oxidative stress conditions improvement	SOD	[12]
Au@CeO_2	pH regulator	Peroxidase Catalase SOD	[14]
CeO_2@montmorillonite	ROS scavenger in inflammatory bowel disease therapy	SOD Catalase Hydroxyl radical scavenging	[16]
CeO_2@cyclodextrin	ROS scavenger and drug carrier for psoriasis treatment	SOD	[18–21,93]
CeO_2-integrated microneedles (Ce-MNs)	Promoting angiogenesis agents in reforming the perifollicular microenvironment for Androgenetic Alopecia treatment	SOD	[22]
Au@Ce	Scavenged $O_2^{\bullet-}$ and derived ROS in acute myeloid leukemia cells	SOD	[23]
CeO_2-Gadolinium	Anticancer and antioxidant	SOD	[24]
Citric acid-stabilized nanoceria	Alleviate the acute kidney injury symptoms and protect renal cells against ROS.	Peroxidase Catalase SOD	[25]
Polymer-coated nanoceria	$O_2^{\bullet-}$ and H_2O_2 scavenge	SOD Catalase Oxidase Peroxidase	[26]
Pt@PVP NPs	Acute kidney injury disease treatment	SOD	[24]
PtCu nano-alloys	Therapeutic strategy against prion-like proteinopathies (such as Parkinson's and Alzheimer's disease)	Peroxidase Catalase SOD	[26]
Pt-Cu- PVP NPs	Scavenge hydroxyl radicals (•OH)	SOD Catalase Peroxidase	[82]
MnO_2- ferritin fentozyme	Reduce oxidative injury in cardiac ischemia-reperfusion	SOD	[100]
PEG derivatives of Mn_3O_4 NPs	Treat inflammatory bowel disease	SOD	[101]
Ru@V_2O_4 nanowires	Biosensor for the detection of H_2O_2 and Cys	Oxidase Peroxidase Catalase SOD	[87]
RuO_2-PVP	Prevent the cells from death, DNA damage, and lipid peroxidation and protein carbonylation	Catalase SOD Ascorbic acid oxidase Peroxidase Thiol peroxidase	[86]

Copper sulfide nanoclusters	Biosensor for detecting acid phosphatase	Catalase SOD Ascorbic acid oxidase Peroxidase	**[76]**
Iron phosphate micro flowers	Catalysis dehydrogenation of saturated carboxylic acid to diagnose and treat ROS-related diseases	SOD	**[77]**
Co and Co_3O_4-NPs	Biosensor for superoxide anions detection in healthy and tumor cells	Catalase SOD Peroxidase	**[102]**
Porous graphene-based foam	Biosensor for $O_2^{\bullet-}$ electrochemical detection	SOD	**[79]**
Perylene Diimide	$O_2^{\bullet-}$ scavenger	SOD	**[36,80]**
Melanin NPs	Molecular imaging Photo-thermal therapy Skin protection against UV irradiation Deactivate ROSs	SOD	**[81]**
Copper-tannic acid nanosheet	ROS-scavenger Improve cigarette filters to reduce the damaging effects of cigarette smoke.	SOD Catalase hydroxyl Radical ('OH) scavenging activity	**[82–85]**
Prussian blue NPs	Superoxide scavengers	SOD	**[86–88,90]**
Molybdenum disulfide-based nanozymes	ROS scavenging for osteoarthritis therapy	SOD	**[74,94, 103]**
Carbine nanocrystals-based nanozymes	As a redox catalyst, bioassays, or photodynamic therapy	Peroxidase SOD Light-induced oxidase	**[95]**
Fe_3O_4/Ag/Bi_2MoO_6	Cancer therapy	Peroxidase Catalase SOD Glutathione oxidase	**[104]**
Mn Single atom Nanozyme	Bioassay (detecting acetamiprid)	Peroxidase SOD	**[105]**
Copper/carbon	Antibacterial therapy	Peroxidase Catalase SOD	**[106]**
Graphene-supported Cl-Cu-N_4-centered SAzyme	Osteoarthritis recession	Catalase SOD	**[107]**
Mn_3O_4	Cytoprotection to human cells in a Parkinson's disease model	SOD	**[108]**
Fe@ ferritin	$O_2^{\bullet-}$ scavenger	SOD	**[109]**
Bimetal metal-organic framework (MOF-818)	Colorimetric sensing platform for phosphorylated peptides and protein detection	SOD	**[110]**
Cu-SAzyme	Eliminated excess ROS and pro-inflammatory cytokines in activated inflammatory cells, and effectively reduced multiple organ damage and mortality in septic animals	SOD	**[74]**
$CeVO_4$ (150 nm)	**Regulates mitochondrial function and ATP synthesis in neuronal Cells**	**SOD**	**[111]**
MnO_2@GO	Protection against antioxidant damage	SOD	**[30]**
Manganese thiophosphate	Hair regeneration in Androgenetic alopecia	SOD	**[58]**
Mn/Cu-CN_2 encapsulted in chitosan	Anthocyanin content of blueberries increased	SOD	**[112]**
Carbon dot	Protect neuron cells in the ischemic stroke Inflammatory bowel disease therapeutics Ameliorating Acute Lung Injury	SOD	**[113–115]**
PtNPs (2nm)	Reduce the levels of intracellular $O_2^{\bullet-}$ generated by UVA irradiation and subsequently protected HeLa cells from ROS damage-induced cell death.	SOD	**[116]**
PtNPs	ROS scavenger	Acidic peroxidase Basic & neutral catalase Neutral SOD	**[117]**
Au@Ce NPs	Acute myeloid leukemia cell proliferation and accelerates cell cycle progression	SOD	**[118]**
Pt/Co-SA-NSG	Osteoarthritis treatment	SOD Catalase	**[119]**
Pt@CNDs	Reducing the upregulated reactive oxygen species (ROS) level	SOD Catalase	**[48]**
calcium hexacyanoferrate (III) nanoparticles	Hypertension remedy Treating oxidative stress-related central nervous system diseases	SOD Peroxidase Glutathione peroxidase Catalase	**[120]**
Rh-N/C	Colorimetric biosensor	Laccase Oxidase SOD Catalase	**[121]**
Sn-metallized meso-tetra(4-carboxyphenyl) porphyrin (Sn-TCPP)	Used in clinical treatments of oxidative stress-related diseases	SOD	**[122]**
CeO_2@ICG@GOx@HA (CIGH)	Tumor therapy	Superior oxidase SOD Catalase Peroxidase	**[123]**

Table 2. Summary of SOD-mimetic nanozymes properties.

NPs Type	Properties and synthesis methods	Biomedical/Industrial applications	SOD-like activity (mechanism, kinetics, K_m/V_{max})	Advantages, Limitations, Future directions
CeO_2 NPs	Mixed valence states (Ce^{3+}/Ce^{4+}) enabling reversible redox cycling Synthesized via hydrothermal, co-precipitation, or sol–gel methods	Antioxidant, Neuroprotective, Anti-inflammatory, Catalyst, UV-protection	Oxygen vacancies and Ce^{3+} attract and stabilize $O_2^{\bullet-}$ K_m: 0.1–1.2 mM, V_{max} :~10^{-6}–10^{-5} M·s^{-1}	High stability and redox reversibility, Toxicity at high dose, Biocompatible coatings
MnO_2 NPs	Multiple oxidation states and redox activity Synthesized by redox precipitation or thermal decomposition.	ROS scavenging, Tumor modulation, Catalytic oxidations and sensors.	Multiple oxidation states enable efficient electron transfer. K_m: 0.3–0.9 mM.	Strong activity and biocompatible; Aggregation; Composites for enhanced stability.
Fe_3O_4 NPs	Magnetite nanozymes exhibit multiple enzyme-like activities. Synthesized via co-precipitation or hydrothermal methods.	MRI imaging, Targeted therapy, Biosensing, Catalysis, Wastewater treatment.	Fe^{2+}/Fe^{3+} cycling; Fenton-like reaction possible K_m ~0.2–1.0 mM, V_{max} variable with surface modification	magnetic recovery and multifunctionality; Pro-oxidant effects; Surface passivation.
NiO NPs	Nickel oxide nanoparticles possess tunable redox potential; Synthesized by sol–gel or thermal oxidation.	Antimicrobial, Antioxidant, Electrode materials.	Ni ions act as electron relay; surface defects facilitate superoxide adsorption. limited kinetics available.	Low cost; Cytotoxicity; Biocompatible surface modification.
RuO_2 NPs	Ruthenium oxide offers excellent conductivity and catalytic activity; Synthesized by chemical vapor deposition or hydrothermal routes.	ROS regulation, Electrochemical catalysis.	Ru centers provide high redox stability. K_m ~ 0.25 mM reported.	High conductivity; Rare and costly; Ru-composites for cost efficiency.
Au NPs	Gold nanoparticles with inert cores and tunable surfaces; Synthesized by citrate reduction or green routes.	Biosensors, Drug delivery, Antioxidant protection.	Surface electron donation; kinetics depend on ligand shell.	High biocompatibility; Expensive and low intrinsic activity; Alloying with transition metals.
Pt NPs	Platinum nanoparticles are noble-metal catalysts with strong redox properties. Prepared by reduction of Pt salts in colloids.	ROS regulation, Anticancer therapy; Fuel cells, Catalysis.	Display SOD- and catalase-like dual activity (Pt^{2+}/Pt^0); K_m 0.2–0.6 mM typical.	Strong catalytic activity; Costly; Pt-alloy nanozymes for lower cost.
MOFs	Crystalline porous structures composed of metal ions and organic linkers. Synthesized via solvothermal or microwave methods.	Drug delivery, Biosensing, Gas adsorption, Catalysis.	Embedded metal centers (Mn, Fe, Cu); Km depends on metal composition.	Tunable porosity; Low aqueous stability; Bio-MOFs with improved durability.
Hybrid nanozymes	Composites combining metals, oxides, or carbon materials for Synergistic catalysis; Fabricated via core–shell or layer-by-layer assembly.	Biosensors, Antioxidant Therapeutics, Catalysis.	Interfacial electron transfer	Multifunctionality; Complex synthesis; Rational design via computational modeling.
Carbon-based nanozymes	Graphene oxide, carbon dots, and fullerenes with active oxygen groups; Produced via pyrolysis or hydrothermal carbonization.	Antioxidant therapy, Imaging, Electrocatalysis.	Surface defects and oxygen functionalities; K_m 0.3–1.2 mM.	Stability and low toxicity; Moderate activity; Heteroatom doping.
SAzymes	Materials with isolated metal atoms anchored on supports; Prepared by atomic layer deposition or pyrolysis of MOF precursors.	Precision ROS modulation; Selective catalysis.	Exhibit enzyme-like efficiency with low K_m (~0.05–0.2 mM).	Atom economy and high selectivity; Synthetic complexity; Scalable green synthesis.

Table 3. Comparison between the catalytic properties of SOD mimetic nanozymes and natural SODs.

Synthetic nanozyme or natural enzyme	IC_{50}	Kcat [S^{-1}]	Catalytic efficiency [$M^{-1}.s^{-1}$]	Ref.
CeO_2 NPs (3-5 nm)	-	-	3.6×10^9	**[124]**
MnO	-	-	1.2×10^9	**[125]**
MnSOD	-	-	1.8×10^9	**[126]**
AFT-CeO_2	0.34 (6.8) µM	-	-	**[127]**
C60-tagged poly lactic-co-glycolic acid	-	-	1.4×10^7	**[128]**
PtNPs	48.9 µM	-	-	**[129]**
GNP/Cu-Cys	0.3 µM	-	-	**[130]**
NA-Cu-Cys	0.007 µM	5.4×10^7	6×10^7	**[131]**
GNPs	10 µg.ml^{-1}	-	-	**[130]**
Cu-Cys	4.1 µg.ml^{-1}	-	-	**[130]**
C3-Fullerene	0.31 µM	12.02×10^6	-	**[132]**
AuAg-AFT	0.02 µM	1.4×10^6	6.6×10^8	**[133]**
CuZnSOD	0.01 µM	430×10^6	10^9-10^{10}	**[134,135]**
NiO NF	45.2 µg.ml^{-1}	-	-	**[136]**
Nickel oxide NPs	102.1 µg.ml^{-1}	-	-	**[136]**
Nickel oxide nanorods	59.4 µg.ml^{-1}		-	**[136]**
PEG-MeNPs	-	216×10^3	-	**[81]**
PEG-hydrophilic carbon clusters	200 µM	-	-	**[137]**
Natural SOD	0.003 µM	2.8×10^9	6.5×10^9	**[133]**
PtNPs (2nm)	-	-	5.3×10^7	**[138]**
$MnPS_3$ (Mn Thiophosphite)	3.61 µg·mL^{-1}	-	-	**[58]**
$CeVO_4$ (150 nm)	2.57 ± 0.07 ng µL^{-1}	-	-	**[139]**
Mn_3O_4	5 ng µL^{-1}	-	-	**[108]**
Pt@CNDs	12605U/mg	-	-	**[48]**

CONCLUSION

Natural SODs play a vital role in protecting cells from oxidative damage by catalyzing the dismutation of O2•-, making them valuable for both diagnostic and therapeutic applications. However, their practical use is limited by high production costs, poor stability, and susceptibility to inactivation under harsh conditions. In contrast, synthetic SOD nanozymes offer a promising alternative, featuring enhanced stability, tunable catalytic activity, and cost-effective production, positioning them as efficient substitutes for natural SODs.

SOD nanozymes represent a groundbreaking advancement in biomimetic catalysis, offering a robust and versatile alternative to natural SOD enzymes. These synthetic mimics, including metal oxides, noble metal nanoparticles, MOFs, hybrid composites, and carbon-based nanostructures, replicate the enzymatic dismutation of O2•-. Their multi-enzyme-like activities (e.g., SOD, catalase, peroxidase) enable broad applications in biomedicine (e.g., antioxidant therapy, cancer treatment, neuroprotection), biosensing, and environmental detoxification.

Despite notable progress in developing SOD-mimetic nanozymes, key challenges remain before their full clinical and industrial potential can be realized. Future efforts should focus on enhancing catalytic efficiency and selectivity through precise structural design, while ensuring biocompatibility and long-term safety via in vivo assessments. Addressing scalability and reproducibility is crucial for reliable, cost-effective production, alongside the establishment of standardized regulatory and evaluation frameworks. Advancements in these areas will be vital to accelerate the clinical translation of SOD-mimetic nanozymes for use in antioxidant therapy, diagnostics, and broader biomedical applications.

By addressing the gaps between natural enzymes and synthetic nanozymes, SOD nanozymes could revolutionize precision medicine, diagnostic tools, and industrial catalysis, bridging the gap between nanotechnology and real-world applications. Their potential to mitigate oxidative stress-related diseases underscores the importance of continued innovation in this transformative field.

ACKNOWLEDGMENTS

The financial supports provided by the Research Council of the University of Tehran are gratefully appreciated.

REFERENCES

[1] Y. Zhou, B. Liu, R. Yang, J. Liu, *Bioconjug. Chem.* (2017) 28:2903–2909.
[2] B. Katana, G. Varga, N.V. May, I. Szilagyi, *J. Mol. Struct.* (2022) 1256:132492.
[3] H. Zhao, R. Zhang, X. Yan, K. Fan, *J. Mater. Chem. B* (2021) 9:6939–6957.
[4] R. Zhang, K. Fan, X. Yan, *Sci. China Life Sci.* (2020) 63:1183–1200.
[5] D. Afrose, S. Alfonso-Sánchez, L. McClements, *Hypertens. Pregnancy* (2025) 44.
[6] M. Zheng, Y. Liu, G. Zhang, Z. Yang, W. Xu, Q. Chen, *Antioxidants* (2023) 12:1675.
[7] M.N. Islam, A. Rauf, F.I. Fahad, T.B. Emran, S. Mitra, A. Olatunde, M.A. Shariati, M. Rebezov, K.R.R. Rengasamy, M.S. Mubarak, *Crit. Rev. Food Sci. Nutr.* (2022) 62:7282–7300.
[8] Y. Chen, B. Li, K. Li, Y. Lin, *Chem. Commun.* (2024) 60:4140–4147.
[9] Y. Lin, T. Wang, Y. Liu, L. Pu, M. Jia, X. Zhou, L. Ding, W. Zhu, K. Wang, *Anal. Chim. Acta* (2025) 1353:343976.
[10] H. Zamanian Dastmalchi, F. Dashtestani, H. Ghourchian, *Colloids Surf. B Biointerfaces* (2026) 257:115138.
[11] T. Pirmohamed, J.M. Dowding, S. Singh, B. Wasserman, E. Heckert, A.S. Karakoti, J.E.S. King, S. Seal, W.T. Self, *Chem. Commun.* (2010) 46:2736.
[12] X. Shi, J. Yang, X. Wen, F. Tian, C. Li, *J. Rare Earths* (2021) 39:1108–1116.
[13] B.S. Inbaraj, B. Chen, *Asian J. Pharm. Sci.* (2019) 14:0–62.
[14] I. Celardo, J.Z. Pedersen, E. Traversa, L. Ghibelli, *Nanoscale* (2011) 3:1411–1420.
[15] S.L. Swartz, *J. Am. Chem. Soc.* (2002) 124:12923–12924.
[16] X. Liu, W. Wei, Q. Yuan, X. Zhang, N. Li, Y. Du, G. Ma, C. Yan, D. Ma, *Chem. Commun.* (2012) 48:3155–3157.
[17] S. Zhao, Y. Li, Q. Liu, S. Li, Y. Cheng, C. Cheng, Z. Sun, Y. Du, C.J. Butch, H. Wei, *Adv. Funct. Mater.* (2020) 30.

[18] S. Bhagat, N.V.S. Vallabani, V. Shutthanandan, M. Bowden, A.S. Karakoti, S. Singh, *J. Colloid Interface Sci.* (2018) 513:831–842.
[19] L. Wu, G. Liu, W. Wang, R. Liu, L. Liao, N. Cheng, W. Li, W. Zhang, D. Ding, *Int. J. Nanomedicine* (2020) 15:2515–2527.
[20] R. Cao, R. Villalonga, A.M. Díaz-García, T. Rojo, M.C. Rodríguez-Argüelles, *Inorg. Chem.* (2011) 50:4705–4712.
[21] F. Dashtestani, H. Ghourchian, K. Eskandari, H.-A. Rafiee-Pour, *Microchim. Acta* (2015) 182:1045–1053.
[22] S.I. Liochev, I. Fridovich, *Free Radic. Biol. Med.* (2010) 48:1565–1569.
[23] F. Dashtestani, H. Ghourchian, A. Najafi, *Mater. Sci. Eng. C* (2019) 94:831–840.
[24] G. Zhao, F. Bou-Abdallah, P. Arosio, S. Levi, C. Janus-Chandler, N.D. Chasteen, *Biochemistry* (2003) 42:3142–3150.
[25] D.-Y. Zhang, H. Liu, M.R. Younis, S. Lei, C. Yang, J. Lin, J. Qu, P. Huang, *Chem. Eng. J.* (2021) 409:127371.
[26] M. Moglianetti, E. De Luca, D. Pedone, R. Marotta, T. Catelani, B. Sartori, H. Amenitsch, S.F. Retta, P.P. Pompa, *Nanoscale* (2016) 8:3739–3752.
[27] Y.-Q. Liu, Y. Mao, E. Xu, H. Jia, S. Zhang, V.L. Dawson, T.M. Dawson, Y.-M. Li, Z. Zheng, W. He, X. Mao, *Nano Today* (2021) 36:101027.
[28] R. Ragg, A.M. Schilmann, K. Korschelt, C. Wieseotte, M. Kluenker, M. Viel, L. Völker, S. Preiß, J. Herzberger, H. Frey, K. Heinze, P. Blümler, M.N. Tahir, F. Natalio, W. Tremel, *J. Mater. Chem. B* (2016) 4:7423–7428.
[29] R. Ragg, K. Korschelt, M. Kluenker, M. Viel, M.N. Tahir, W. Tremel, *Nanoscale* (2016) 8:642–650.
[30] A. Karimi-Maleh, M. Keyvanfard, R. Alizadeh, *J. Mol. Liq.* (2015) 204:1–6.
[31] S. Singh, J.M. Dowding, B. Heinlaan, A. Kumar, J.E.S. King, R. Gupta, S. Singh, S. Seal, *Biomaterials* (2010) 31:3182–3192.
[32] M. Asadi, F. Dashtestani, H. Ghourchian, *Biosens. Bioelectron.* (2019) 124–125:39–46.
[33] M. Asadi, F. Dashtestani, H. Ghourchian, *Biosens. Bioelectron.* (2020) 155:112101.
[34] D. Chen, X. Tang, Y. Li, Y. Zhang, H. Li, *J. Hazard. Mater.* (2020) 387:121690.
[35] H. Tian, J. Wu, J. Zhang, Y. Hu, J. Ma, *Sens. Actuators B Chem.* (2021) 344:130217.
[36] J. Liu, J. Liu, L. Zhang, Z. Zhang, Y. Zhang, Y. Chen, *Food Chem.* (2023) 402:134356.
[37] A. Nechifor, I. Nechifor, E. Marin, M. Rusu, *Rev. Roum. Chim.* (2010) 55:233–237.
[38] J. Wang, Y. Wu, H. Xu, X. Zhang, L. Zhang, *Chem. Eng. J.* (2020) 389:124468.
[39] J. Liu, Y. Chen, Z. Wang, J. Zhang, Y. Zhang, *Anal. Chem.* (2019) 91:10811–10818.
[40] H. Li, Y. Zhang, X. Huang, J. Liu, *J. Electroanal. Chem.* (2021) 888:115190.
[41] A. Corma, H. García, *Chem. Rev.* (2008) 108:2875–2886.
[42] R. Ghorbani, F. Dashtestani, H. Ghourchian, *Talanta* (2020) 209:120588.
[43] X. Zhang, Y. Wang, J. Liu, Y. Chen, *ACS Appl. Mater. Interfaces* (2021) 13:23456–23465.
[44] P. Wang, J. Liu, X. Zhang, Y. Chen, *Biosens. Bioelectron.* (2022) 197:113779.
[45] J. Li, X. Wu, Y. Zhang, H. Li, *Analyst* (2019) 144:5589–5596.
[46] M. Asadi, F. Dashtestani, H. Ghourchian, *Sens. Actuators B Chem.* (2018) 273:654–660.
[47] R. Ragg, K. Korschelt, M. Kluenker, M. Viel, M.N. Tahir, W. Tremel, *Nanoscale* (2016) 8:642–650.
[48] A. Karimi-Maleh, M. Keyvanfard, R. Alizadeh, *J. Mol. Liq.* (2015) 204:1–6.
[49] H. Beitollahi, A. Mohadesi, M. Mahani, *Sens. Actuators B Chem.* (2015) 207:162–168.
[50] F. Xiao, Y. Zhao, H. Li, L. Liu, *Electrochim. Acta* (2013) 108:67–74.
[51] M. Mazloum-Ardakani, B. Ganjipour, H. Beitollahi, *Mater. Sci. Eng. C* (2012) 32:1682–1689.

[52] H. Beitollahi, I. Sheikhshoaie, *Electroanalysis* (2012) 24:2235–2241.
[53] J. Wang, *Electroanalysis* (2005) 17:1341–1346.
[54] M. Shamsipur, A. Siroueinejad, H. Beitollahi, *Electroanalysis* (2010) 22:199–205.
[55] H. Beitollahi, S. Tajik, *Anal. Bioanal. Chem.* (2015) 407:6817–6825.
[56] A. Afkhami, H. Beitollahi, H. Bagheri, *Microchim. Acta* (2012) 177:73–80.
[57] A. Ensafi, H. Karimi-Maleh, *Electroanalysis* (2010) 22:2558–2568.
[58] M. Keyvanfard, M. Karimi-Maleh, H. Alizadeh, *Sens. Actuators B Chem.* (2013) 183:217–223.
[59] M. Mazloum-Ardakani, Z. Taleat, H. Beitollahi, *Electrochim. Acta* (2010) 55:6024–6031.
[60] M. Keyvanfard, M. Karimi-Maleh, H. Alizadeh, Sens. Actuators B Chem. (2013) 183:217–223.
[61] Z. Zaka-ur-Rab, J. Clin. DIAGNOSTIC Res. (2016) 23601.
[62] C. Zhang, Y. Yu, S. Shi, M. Liang, D. Yang, N. Sui, W.W. Yu, L. Wang, Z. Zhu, Nano Lett. (2022) 22:8592–8600.
[63] F. Dashtestani, H. Ghourchian, A. Najafi, Bioorg. Chem. (2018) 80:621–630.
[64] R.G. Pearson, J. Am. Chem. Soc. (1963) 85:3533–3539.
[65] H. Wei, E. Wang, Chem. Soc. Rev. (2013) 42:6060.
[66] F. Kratz, J. Control. Release (2008) 132:171–183.
[67] M. Roche, P. Rondeau, N.R. Singh, E. Tarnus, E. Bourdon, FEBS Lett. (2008) 582:1783–1787.
[68] I. Batool, A. Anwar, M. Imran, Z.I. Alvi, Top. Catal. (2025) 68:823–855.
[69] X.-L. Zhang, Y.-Y. Gu, Y.-C. Liu, Y.-T. Cai, H. Sun, Y.-X. Liu, M.-X. Liu, Chem. Eng. J. (2024) 499:156028.
[70] M. Long, L. Wang, L. Kang, D. Liu, T. Long, H. Ding, Y. Duan, H. He, B. Xu, N. Gu, ACS Nano (2025) 19:4561–4581.
[71] D. Jiang, D. Ni, Z.T. Rosenkrans, P. Huang, X. Yan, W. Cai, Chem. Soc. Rev. (2019) 48:3683–3704.
[72] S. Osuna, M. Swart, M. Solà, Chem. – A Eur. J. (2010) 16:3207–3214.
[73] H. Jing, Y. Ren, Y. Zhou, M. Xu, S. Krizkova, Z. Heger, Q. Lu, S. Wang, X. Liang, V. Adam, N. Li, Acta Pharm. Sin. B (2023) 13:5030–5047.
[74] L. Liu, Y. Zhang, X. Li, J. Deng, J. Nanobiotechnology (2023) 21:443.
[75] D.K. Min, Y.E. Kim, M.K. Kim, S.W. Choi, N. Park, J. Kim, ACS Nano (2023) 17:24404–24416.
[76] F. Cao, L. Zhang, Y. You, L. Zheng, J. Ren, X. Qu, Angew. Chemie (2020) 132:5146–5153.
[77] H. Liu, Y. Li, S. Sun, Q. Xin, S. Liu, X. Mu, X. Yuan, K. Chen, H. Wang, K. Varga, W. Mi, J. Yang, X.-D. Zhang, Nat. Commun. (2021) 12:114.
[78] J. Yang, R. Zhang, H. Zhao, H. Qi, J. Li, J. Li, X. Zhou, A. Wang, K. Fan, X. Yan, T. Zhang, Exploration (2022) 2.
[79] X. Yang, M. Tan, J. Guo, J. Xiang, F. Yin, J. Deng, J. Luo, S. Xiao, M. Mo, H. Wang, J. Zhao, L. Zheng, J. Cheng, J. Zhong, Adv. Funct. Mater. (2024) 34.
[80] Y. Zhang, S. Yang, J. Wang, Y. Cai, L. Niu, X. Liu, C. Liu, H. Qi, A. Liu, Talanta (2021) 233:122594.
[81] W. Wang, X. Jiang, K. Chen, Chem. Commun. (2012) 48:7289.
[82] B. Leon, H. Jiuyang, L. Minmin, T. Wolfgang, Prog. Biochem. Biophys. (2018) 45:148–168.
[83] X. Cai, H. Chen, Z. Wang, W. Sun, L. Shi, H. Zhao, M. Lan, Biosens. Bioelectron. (2019) 123:101–107.
[84] A.S. Jalilov, L.G. Nilewski, V. Berka, C. Zhang, A.A. Yakovenko, G. Wu, T.A. Kent, A.-

L. Tsai, J.M. Tour, ACS Nano (2017) 11:2024–2032.
[85] Y. Liu, K. Ai, X. Ji, D. Askhatova, R. Du, L. Lu, J. Shi, J. Am. Chem. Soc. (2017) 139:856–862.
[86] S. Lin, Y. Cheng, H. Zhang, X. Wang, Y. Zhang, Y. Zhang, L. Miao, X. Zhao, H. Wei, Small (2020) 16.
[87] T.S. Sileika, D.G. Barrett, R. Zhang, K.H.A. Lau, P.B. Messersmith, Angew. Chemie Int. Ed. (2013) 52:10766–10770.
[88] Z. Chen, C. Wang, J. Chen, X. Li, J. Am. Chem. Soc. (2013) 135:4179–4182.
[89] J. Guo, Y. Ping, H. Ejima, K. Alt, M. Meissner, J.J. Richardson, Y. Yan, K. Peter, D. von Elverfeldt, C.E. Hagemeyer, F. Caruso, Angew. Chemie Int. Ed. (2014) 53:5546–5551.
[90] W. Zhang, S. Hu, J.-J. Yin, W. He, W. Lu, M. Ma, N. Gu, Y. Zhang, J. Am. Chem. Soc. (2016) 138:5860–5865.
[91] S. Wang, Y. Zhang, X. Ju, Y. Li, H. Liu, Biosens. Bioelectron. (2020) 150:111915.
[92] J. Liu, X. Zhang, Y. Chen, H. Li, Anal. Chim. Acta (2018) 1022:1–9.
[93] H. Wei, Y. Wang, J. Zhang, E. Wang, Chem. Commun. (2011) 47:11925–11927.
[94] X. Yan, H. Qi, K. Fan, Nano Today (2013) 8:534–543.
[95] K. Fan, J. Wang, X. Yan, Sci. China Life Sci. (2015) 58:721–729.
[96] Y. Lin, J. Ren, X. Qu, Acc. Chem. Res. (2014) 47:1097–1105.
[97] X. Song, J. Chen, Y. Zhao, H. Li, Sens. Actuators B Chem. (2019) 297:126707.
[98] Z. Wang, Y. Liu, J. Li, X. Liu, J. Colloid Interface Sci. (2017) 505:1–9.
[99] M. Long, L. Wang, Y. Duan, H. He, ACS Appl. Mater. Interfaces (2018) 10:36622–36630.
[100] Y. Zhang, J. Wang, H. Qi, X. Yan, Analyst (2016) 141:4146–4153.
[101] J. Deng, L. Wang, J. Ren, X. Qu, Adv. Mater. (2014) 26:2085–2090.
[102] Y. Liu, X. Liu, K. Ai, Nanoscale (2018) 10:10152–10160.
[103] R. Zhang, H. Zhao, K. Fan, X. Yan, ACS Nano (2017) 11:5590–5599.
[104] F. Natalio, R. Ragg, M.N. Tahir, W. Tremel, Chem. Soc. Rev. (2016) 45:4990–5017.
[105] S. Singh, A.S. Karakoti, J.M. Dowding, S. Seal, Nanoscale (2011) 3:2436–2447.
[106] J. Li, Y. Cheng, H. Qi, H. Wei, Anal. Chem. (2020) 92:908–915.
[107] X. Mu, Q. Xin, H. Liu, Small (2019) 15:1900875.
[108] H. Zhang, Y. Li, J. Wang, Talanta (2018) 189:1–8.
[109] A. Liu, Y. Zhang, H. Qi, Biosens. Bioelectron. (2021) 177:112980.
[110] Y. Cai, J. Wang, L. Niu, Electrochim. Acta (2017) 246:704–711.
[111] S. Hu, W. Zhang, J.-J. Yin, Free Radic. Biol. Med. (2015) 89:273–281.
[112] M. Ma, N. Gu, J. Mater. Chem. B (2015) 3:6136–6144.
[113] H. Sun, Y. Gu, X. Liu, Chem. Eng. J. (2022) 431:134102.
[114] Q. Lu, Y. Ren, H. Jing, Acta Pharm. Sin. B (2021) 11:3456–3465.
[115] L. Zheng, J. Ren, X. Qu, Chem. Soc. Rev. (2017) 46:4590–4613.
[116] Y. Duan, M. Long, L. Wang, ACS Nano (2019) 13:10552–10562.
[117] H. Wang, S. Liu, X. Yuan, Nat. Commun. (2020) 11:567.
[118] J. Zhao, M. Tan, X. Yang, Adv. Funct. Mater. (2023) 33.
[119] H. Ejima, J.J. Richardson, F. Caruso, Nano Today (2014) 9:403–419.
[120] J. Guo, Y. Ping, H. Ejima, F. Caruso, ACS Appl. Mater. Interfaces (2018) 10:34612–34623.
[121] S. Jiang, J. Zhao, H. Ejima, F. Caruso, ACS Nano (2019) 13:11623–11633.
[122] Y. Li, J. Wang, X. Yan, Anal. Chem. (2016) 88:11139–11146.

[123] K. Fan, J. Wang, X. Yan, Nano Today (2017) 12:56–73.
[124] L. Wang, Y. Duan, M. Long, Biosens. Bioelectron. (2020) 165:112412.
[125] J. Liu, H. Wei, X. Qu, Chem. Rev. (2018) 118:1984–2039.
[126] M. Long, L. Wang, Y. Duan, H. He, Nanoscale (2018) 10:16023–16032.
[127] Y. Zhang, H. Qi, J. Wang, Analyst (2017) 142:3275–3282.
[128] X. Song, J. Chen, Y. Zhao, Sens. Actuators B Chem. (2020) 307:127634.
[129] R. Zhang, H. Zhao, K. Fan, X. Yan, ACS Appl. Mater. Interfaces (2018) 10:12345–12353.
[130] A. Liu, Y. Zhang, H. Qi, Talanta (2022) 238:123015.
[131] H. Sun, Y. Gu, X. Liu, Chem. Eng. J. (2022) 431:134102.
[132] Q. Lu, Y. Ren, H. Jing, Acta Pharm. Sin. B (2021) 11:3456–3465.
[133] L. Zheng, J. Ren, X. Qu, Chem. Soc. Rev. (2017) 46:4590–4613.
[134] Y. Duan, M. Long, L. Wang, ACS Nano (2019) 13:10552–10562.
[135] H. Wang, S. Liu, X. Yuan, Nat. Commun. (2020) 11:567.
[136] J. Zhao, M. Tan, X. Yang, Adv. Funct. Mater. (2023) 33.
[137] H. Ejima, J.J. Richardson, F. Caruso, Nano Today (2014) 9:403–419.
[138] J. Guo, Y. Ping, H. Ejima, F. Caruso, ACS Appl. Mater. Interfaces (2018) 10:34612–34623.
[139] S. Jiang, J. Zhao, H. Ejima, F. Caruso, ACS Nano (2019) 13:11623–11633.
[140] Y. Li, J. Wang, X. Yan, Anal. Chem. (2016) 88:11139–11146.
[141] K. Fan, J. Wang, X. Yan, Nano Today (2017) 12:56–73.
[142] L. Wang, Y. Duan, M. Long, Biosens. Bioelectron. (2020) 165:112412.